*Radio Science*, Volume 23, Number 3, Pages 347–361, May–June 1988

# Analysis and interpretation of spaced receiver scintillation data recorded at an equatorial station

*D. E. Spatz, S. J. Franke, and K. C. Yeh*

*Department of Electrical and Computer Engineering, University of Illinois at Urbana-Champaign*

(Received September 24, 1987; revised February 3, 1988; accepted February 15, 1988.)

Ultrahigh frequency satellite signals from the Pacific FleetSat (53° elevation angle) and *L* band signals from the Pacific Marisat (50° elevation angle) were recorded in Guam, an equatorial station, from April 1982 through May 1, 1983. Three receivers aligned in the magnetic east-west direction were used, with the most widely separated receivers (457.2 m separation) recording the UHF signal amplitudes and the middle receiver recording the *L* Band signal amplitudes. These data are analyzed for the drift characteristics of ionospheric irregularities. The digitized spaced receiver data are processed to yield the scintillation index, the cross-correlation function and the self-power spectrum. By assuming a locally frozen flow, several methods have been devised to compute the drift velocity, $V_0$, and the characteristic random velocity, $V_C$. These methods seem to show internal agreement. They also show that the velocity fluctuations decrease markedly during the first few hours after local sunset. The spectral index of the self-power spectrum roll-off was also determined during times of both weak and strong scintillation. For the weak scintillation cases, the slopes were observed to gradually steepen as the night progressed into the postmidnight period. This steepening suggests the decaying of smaller-sized irregularities. There were a few exceptions to this observed decay. For the strong scintillation cases, the shape and slope of the self-power spectrum were observed to be influenced by the drift velocity and scattering strength of the irregularities.

## 1. INTRODUCTION

Scintillation due to spatial and temporal variations in the electron density has been observed on radio signal paths through the ionosphere at frequencies ranging from 10 MHz to 6 GHz. Scintillations can cause a signal's amplitude or phase to fluctuate about its mean level because the signal's electromagnetic energy is scattered and redistributed by the disturbed ionospheric *F* region. The occurrence of scintillations has been studied for several decades and its morphology has been documented extensively for the auroral, midlatitude and equatorial regions [Aarons, 1977, 1982]. The most intense scintillations have been observed in the nighttime equatorial region, which is the area that will be studied in this investigation. The electron density variations called "irregularities," ranging in scale size from several kilometers to a few meters, are known to coexist in the postsunset equatorial *F* region [Basu et al., 1978]. In addition to patches of irregularities, discrete irregularity structures which extend to the topside ionosphere, known as "plumes," and very large, spatially abrupt bite-outs, known as "bubbles," have been detected in the nighttime *F* region [Basu et al., 1980]. Although the exact mechanism that triggers the irregularity development is unknown at this time, there is experimental indication that, after local sunset, the bottomside *F* region is subjected to a number of potentially destabilizing stresses (e.g., Rayleigh-Taylor instability, nonlinear **ExB** forces, and velocity shear) causing an upwelling of low electron density plasma into altitudes with higher-density plasma [Ossakow, 1981; Valladeres et al., 1983]. Various sized



Paper number 8S0138.
0048-6604/88/008S-0138$08.00

irregularities may then branch off from the upwelled plasma creating variations in the higher-density plasma.

The ionospheric irregularities are constantly in motion, due to the presence of neutral air winds and electric and magnetic fields. Through spaced receiver and incoherent backscatter techniques, the equatorial irregularities have been found to drift in the magnetic east-west direction, with a vertical component of drift present as well [Woodman, 1970; Paulson, 1984]. The drift velocities just after local sunset may vary considerably from the post-midnight velocities. Measured drift velocities of up to 220 m/s eastward in the early evening hours and 100 m/s westward in the morning hours have been reported at the magnetic equator [Paulson, 1984].

Signals from the UHF channel (250.55 MHz) of the Pacific Ocean Fleet Satellite (0.00°N, 176.50°E) were received by the Naval Communication Area Master Station (12.4°N, 147.0°E) at Guam, on two circularly polarized, helical antennas separated by 457.2 m in the magnetic east-west direction. In addition, the *L* band beacon signal (1.54 GHz) of the Pacific Ocean Maritime Satellite (0.00°N, 179.00°E) was monitored with a receiver in the center of the two helical antennas. The elevation angle of the Pacific Ocean Fleet Satellite as viewed from the receiver was 53.1°, which placed the 400-km subionospheric point at 11.50°N and 149.50°E. The elevation angle of the Pacific Ocean Maritime Satellite was 50.5°. The automatic gain control (AGC) signals at the receivers were brought back to a central point on buried coaxial cables and were recorded on three channels of an analog magnetic tape recorder. The analog data were later calibrated back into amplitude signals and digitized at 12.5 times per second for periods when the UHF signals showed fluctuations. The three channels of digitized amplitude data (east, west and *L* band), along with a time and date code, were then stored in a special format on magnetic tapes. Data for the period from late April 1982 through May 1983 were stored in 97 magnetic tapes. Some of these data have been previously published. For example, Paulson [1984] deduced the drift velocity using the spaced receiver data. On the other hand, Vacchione et al. [1987] applied the correlation analysis to the data and obtained the characteristic random velocity in addition to the drift velocity. They further showed the consistency of the scintillation data with the scintillation theory by using a locally frozen flow model and interpreting the characteristic random velocity as a measure of the rms velocity fluctuations encountered along the propagation path, at least under the weak scatter conditions. They also presented evidence showing that the rms velocity fluctuation is relatively large just after local sunset (on the order of 40 to 50 m/s) and decreases sharply in the postsunset to premidnight period.

In the following section, section 2, are discussed data processing and analysis. The results are interpreted in section 3. The paper is concluded in section 4.

## 2. DATA PROCESSING AND ANALYSIS

The scintillation data can be processed to yield several quantities of interest. The foremost of these is probably the scintillation index $S_4$. Other useful quantities include the autocorrelation function, the cross-correlation function and the spectrum. Some of these quantities can be further related to physical quantities of interest such as drift speed, spectral index, etc. This section is concerned with data processing for physical intepretation.

The scintillation index, $S_4$, is defined as the standard deviation of the intensity divided by the mean or

$$S_4 = \frac{\sqrt{\langle A^4 \rangle - \langle A^2 \rangle^2}}{\langle A^2 \rangle} \tag{1}$$

Here A represents the amplitude and the brackets in the above equation represent time averaging. The $S_4$ index is a measure of the extent of signal fluctuations due to the presence of ionospheric irregularities. For this analysis, an $S_4$ index value of 0.5 or less will distinguish weak scattering from strong scattering. Typically, $S_4$ is calculated and plotted versus local standard time (LST) for every 3 min of east, west and *L* band data.

Each 3-min long data segment (2250 data points) was tested for stationarity. When deemed stationary, the segment was processed using an automated power spectrum program based on the spectral estimation method described by Welch [1967]. The program consisted of breaking up the first 2048 data points of each 2250-point segment into seven overlapping 512-point segments. The overlap consisted of 256 data points. The 512-point data segments were then detrended to remove the mean and linear trends and windowed with a Hanning window function. Each of the seven segments was then input into a 512-point fast Fourier transform routine and the seven results were averaged together leaving one 512-point spectral estimate.

The cross-correlation function is obtained by processing the data according to the following scheme:

$$B(\tau,\Delta x) = F^{-1}\{F(A_1)\bullet F^*(A_2)\} \quad (2)$$

where F and $F^{-1}$ denote the forward and inverse Fourier transform, and F* denotes the complex conjugate of the forward Fourier transform. The expressions $A_1$ and $A_2$ denote the east and west receiver data segments, respectively, normalized to zero mean and unit variance. The autocorrelation function, $B(\tau,0)$, was calculated by averaging $F^{-1}\{F(A_1)\cdot F^*(A_1)\}$ and $F^{-1}\{F(A_2)\cdot F^*(A_2)\}$. These correlation functions are useful in studying the evolution of diffraction patterns to be discussed in the following.

One of the earliest methods devised to measure the variations in the diffraction pattern using spaced receivers was Briggs' "full correlation analysis" [Briggs et al., 1950]. The method involves determining the point of intersection between the temporal autocorrelation function, $B(\tau,0)$, and the temporal cross-correlation function, $B(\tau,\Delta x)$, for two coinciding signals at receivers separated by some distance, $\Delta x$. As discussed by Vacchione et al. [1987], there are three methods that can be used to analyze the data. The first two rely on the assumption that the cross-correlation function $B(t,\Delta x)$ has an ellipsoidal form. In the first method the time, $\tau_b$, where the two cross sections of the space-time correlation functions are equal or $B(\tau_b,0) = B(\tau_b, \Delta x)$ must be determined for a given receiver separation distance $\Delta x$. One can then determine the mean drift velocity, $V_0$, of the diffraction pattern from the equation.

$$V_0 = \frac{\Delta x}{2\tau_b} \quad (3)$$

The second method uses the time, $\tau_p$, where the temporal autocorrelation function is equal to the peak of the temporal cross-correlation function or $B(\tau_p,0)=B(\tau_m,\Delta x)$. This method, sometimes known as the peak value method, uses points closer to the maxima of the correlation functions where the Briggs assumption of elliptical contours is more sound. The expression for the mean drift velocity $V_{02}$ using this method is

$$V_{02} = \frac{\Delta x\bullet\tau_m}{\tau_p^2 + \tau_m^2} \quad (4)$$

The third method used to determine the mean drift velocity is based on the "midpoint method," developed by Coles and Maagoe [1972] to measure solar wind velocities using interplanetary scintillation. The midpoint method takes into account the skewing of the temporal cross-correlation function due to the random time changes in the diffraction pattern. The method uses the times, $\tau_{0.5}{}^1$ and $\tau_{0.5}{}^2$, where the cross-correlation function is at 50% of its maximum value. The method is purely qualitative and has no theoretical basis, but in a past investigation by Vacchione et al. [1987], the measured drift velocities using the midpoint method were in reasonable agreement with the first two methods. Thus, this method will be used in this investigation also. The expression for the mean drift velocity using this method becomes

$$V_{03} = \frac{\Delta x\bullet\tau_m}{(\tau_{0.5}{}^1 + \tau_{0.5}{}^2)} \quad (5)$$

Once the drift velocity is determined by either (3), (4), or (5), its value can be substituted into the following equation to yield a value of the characteristic random velocity.

$$V_C = \sqrt{\frac{\Delta x\bullet V_0}{\tau_m} - V_0{}^2} \quad (6)$$

Experimentally, $V_0$ values determined by these three methods are found to differ by no more than a few percent, but they can cause $V_C$ values to differ by as much as 50%. On occasion the quantity under the radical in (6) can even become negative, yielding a physically meaningless imaginary $V_C$. When this happens, the imaginary $V_C$ values are discarded. Originally, Briggs introduced $V_C$ in his study of varying diffraction patterns on the ground as a characteristic random velocity. As such, $V_C$ was the ratio of the characteristic length and time scales that would be sensed by an observer moving with the average drift velocity of the pattern ($V_0$). Applying the weak scintillation theory, Wernik et al. [1983] and Vacchione et al. [1987] have shown that $V_C$ can be interpreted as the root-mean-square velocity fluctuations, $\sigma_v$, in a locally frozen flow. The scintillation theory has therefore linked $V_C$ to the process occurring in the random ionosphere.

It should be noted that, in the presence of a vertically upward component of drift, the measured drift velocity, $V_0$, is related to the magnetic eastward drift, $V_E$, and the upward component of drift, $V_Z$, by the relation

$$V_0 = V_E - V_Z \tan\theta \sin\phi \quad (7)$$

where $V_E$ is magnetic eastward drift, $V_Z$ is vertically upward drift velocity, $\theta$ is the zenith angle of satellite to station ray path, and $\phi$ is the azimuth angle of satellite to station ray path. For our experimental configuration, $\theta = 36.9°$ and $\phi = 110°$, so that

$$V_0 = V_E - 0.7\, V_Z \quad (8)$$

This relation indicates that due to the slanted line-of-sight paths of the signals, the zonal drift velocity value, $V_E$, may be contaminated in the presence of vertical drift. Thus the contribution of the vertical velocity, $V_Z$, must be included when making interpretations involving the measured mean drift velocity, $V_0$, or the random velocity $V_C$.

## 3. RESULTS AND INTERPRETATION

Figure 1 shows the measured drift velocities for four nights. Only the velocities derived by the peak value method are shown because in a past investigation by Vacchione et al. [1987], the drift velocity values using each of the three correlation methods were shown to be consistently within 5% rms deviation of each other. From Figure 1, it is observed that very sharp increases in the drift velocity can occur just after scintillation onset. As seen in (8), these sharp increases in the measured drift velocity, $V_0$, could be due to either a sudden increase in the eastward drift or the reversal of an upward drift to a downward vertical drift of the irregularities. Radar experiments of Woodman [1970] have shown that the upward vertical drift immediately following the local sunset would drive the ionization to great heights to be followed by a quick downward drift. Vertical velocities as high as 40 m/s upward soon followed by downward velocities as high as 40 m/s were reported. If this maximum reversal of 80 m/s occurs in a matter of minutes with no change in the eastward drift velocity, then by using (7), this would result in sharp increases as high as 56 m/s in the measured drift velocity values. Thus the trend seen in Figure 1 may be consistent with Woodman's observations although the relative importance of the horizontal zonal drift and the vertical velocity cannot be untangled by using the spaced receiver data alone.

Figures 2 and 3 show some experimental results for two of the days shown in Figure 1. Scintillation for many days frequently commenced within an hour of local sunset (typically 1900–2000 LST). As often observed, $S_4$ rose suddenly to nearly saturated levels at UHF. For some nights, the scintillation pattern would indicate a multiple-patch geometry as shown, for example, in Figure 3 for April 23, 1983. It is interesting to note that on this day during the dip in $S_4$ from about 2300 to 0030 LST, the drift as shown in Figure1 did not show any unusual behavior except that it was declining steadily. The magnitude of the random velocity, $V_C$, was calculated using the three methods described in section 2. Invariably, the values computed by the peak value method, depicted in the middle panel of Figures 2 and 3, show less scatter of points and more consistency. This observation would suggest that the peak value method is more reliable than the other two methods. The magnitude of the characteristic random velocity, $V_C$, denoted by a plus sign in the figures, appears to be dependent upon local time. A much larger $V_C$ is observed during the onset phase (within an hour or two after local sunset), when compared to the $V_C$ values at later times. As the night progresses, $V_C$ is observed to decrease. Superposed on this strong local time dependence of $V_C$, our data also suggest a weaker rise of $V_C$ near the boundary of a patch. This behavior is clearly revealed on the western wall of the patch from 0100 to 0200 LST of Figure 2. In the two-patch observation of Figure 3, this rise can also be seen on the western wall of the first patch shortly after 2300 LST and on both the eastern wall and western wall of the second patch. Figure 4 is a composite plot for eight nights when scintillation commenced within an hour of local sunset regardless of its intensity. This plot shows the decaying trend of the characteristic random velocity as a function of local time. Although the three correlation methods used in this analysis determine somewhat different $V_C$ values, they are in agreement as to its decay.

It should be noted that the $V_C$ parameter as originally proposed by Briggs et al. [1950] was a phenomenological parameter and its physical interpretation in terms of temporal rearrangement of ionospheric irregularities was not clear. Recently, however, Wernik et al. [1983] and Vacchione et al. [1987] have applied the theory for weak scintillation to show that the $V_C$ parameter is closely related to two possible mechanisms that cause the observed diffraction patterns to exhibit random time variations. One model proposed by Wernik et al. introduces temporal rearrangement by assuming that the velocity field in the ionosphere can be characterized by a normal distribution of velocities. Under the assumption that the spatial correlation scale of the velocity field is at least as large as the correlation

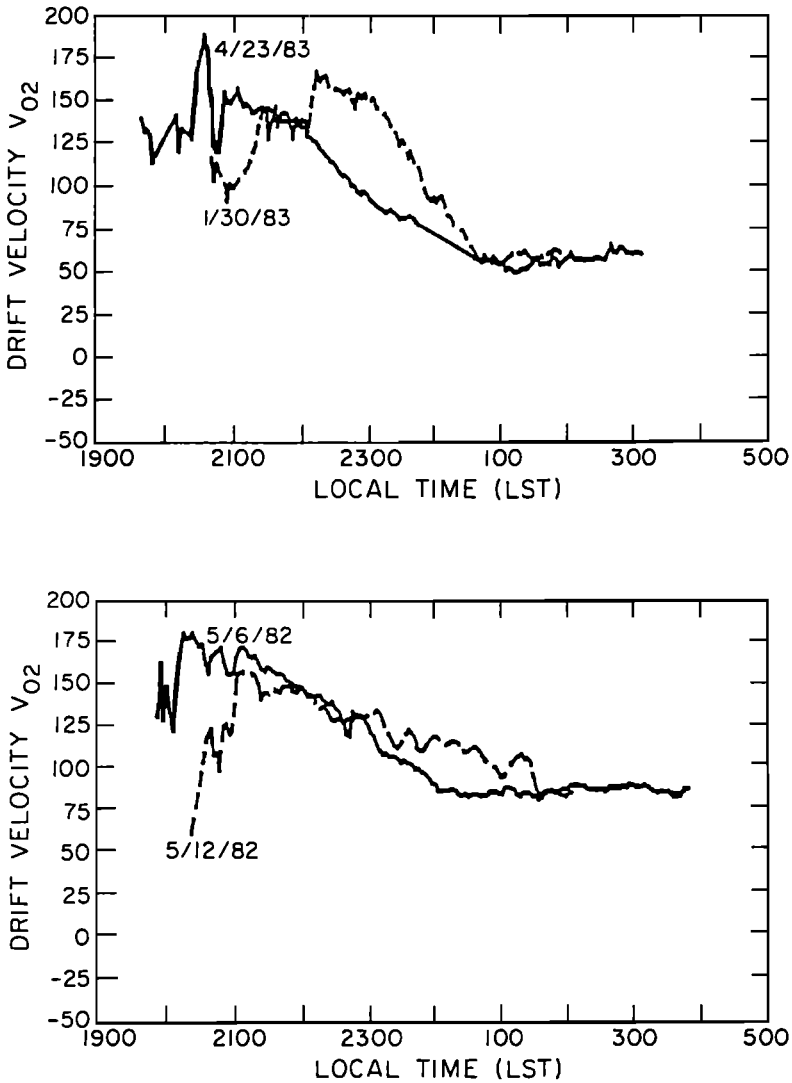


Fig. 1. Measured drift velocities for four nights using the peak value method.

scale of the electron density irregularities, it was shown that $V_C$ is a measure of the width of the velocity distribution ($\sigma_v$). The assumption about the correlation scale of the velocity field is known as the "locally frozen" hypothesis. Vacchione et al. showed that least squares fitting of observed correlation functions to the model developed by Wernik et al. yields estimates for the random velocity spread, $\sigma_v$, that are reasonably consistent with the $V_C$ parameter obtained from classical analysis.

On the other hand, a purely deterministic model can be considered in which, for example, the velocity in the ionosphere exhibits a velocity shear. In this case it was shown that $V_C$ is a measure of the velocity change along the ray path through the height region that contains scintillation producing irregularities.

Both the deterministic shears and more random velocity distributions are observed in the equatorial *F* region. Recent radar interferometer observations of equatorial *F* region drift variability during spread *F* conditions were reported by Kudeki and Franke [1986]. These observations show that large horizontal velocity fluctuations are seen on time scales as short as a few minutes. The vertical scale size of the velocity field was found to be as small as

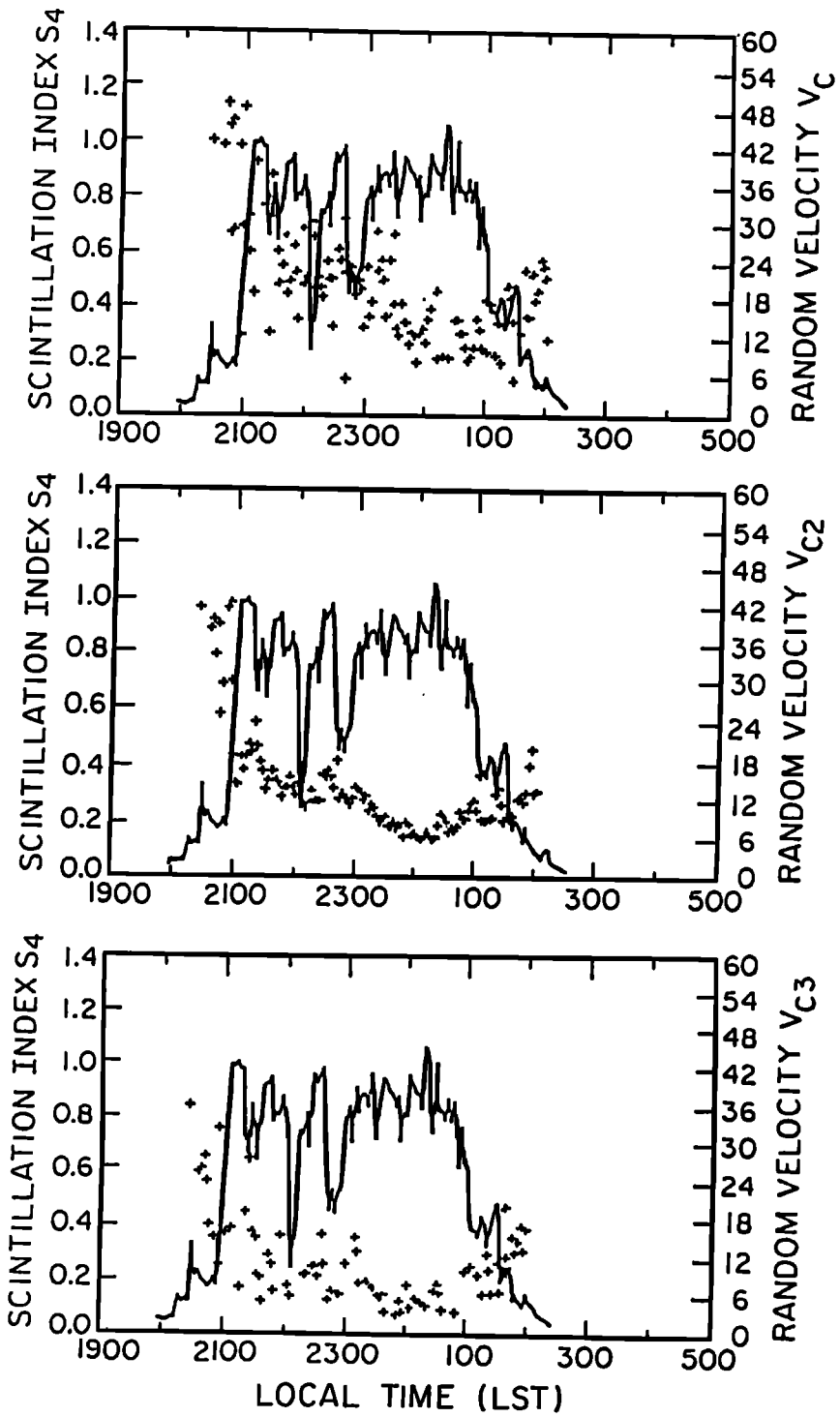


Fig. 2. Random velocity measurements for May 12, 1982. The scintillation index, $S_4$ (dark line, left scale), represents the average of scintillation at the east and west UHF receivers. The characteristic random velocities, $V_C$ (denoted by pluses, right scale) are derived by each of the three methods described in section 2. The units for $V_C$ are meters per second.

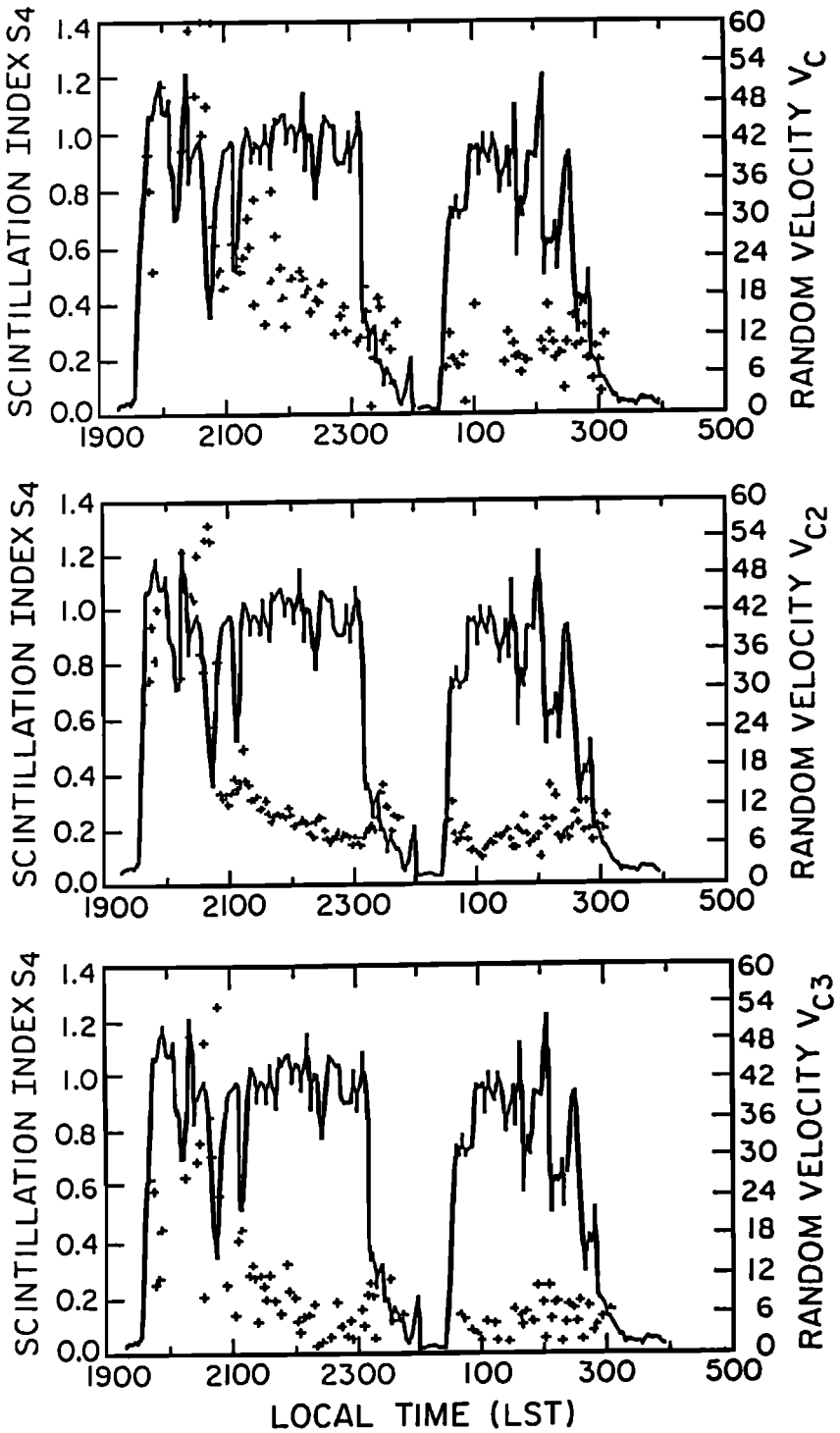


Fig. 3. Random velocity measurements for April 23, 1983. Same units and symbols as in Figure 2.

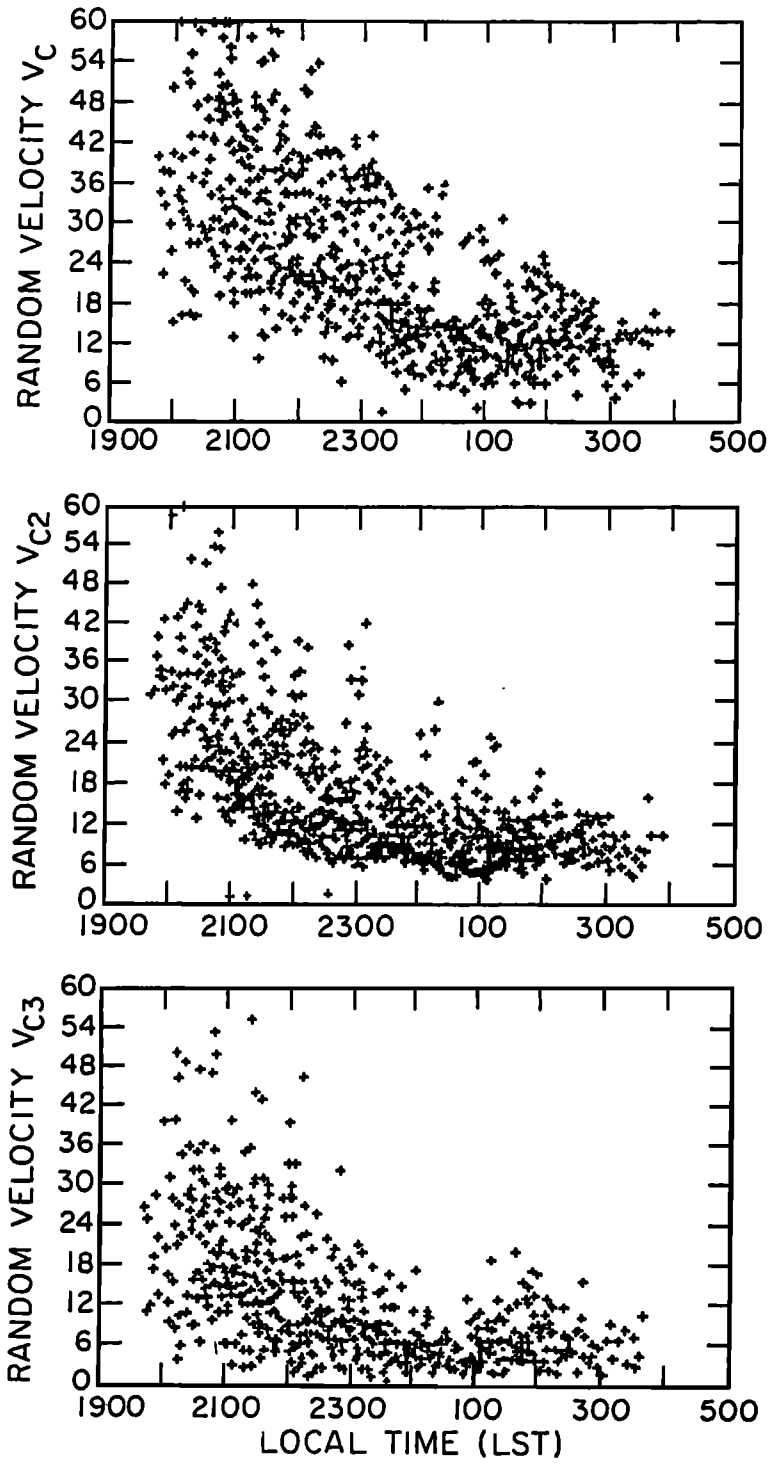


Fig. 4. Random velocity measurements for eight nights of data where scintillation commenced within an hour of local sunset.

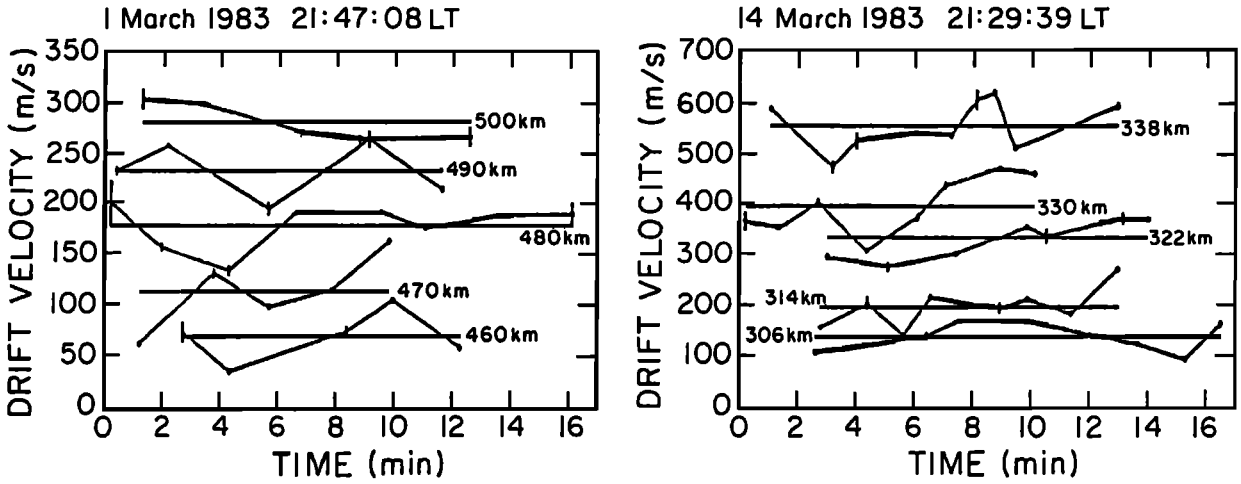


Fig. 5. Summary of drift velocity measurements during spread $F$ conditions using radar interferometry at Jicamarca, Peru [Kudeki and Franke, 1986]. See Table 1. The two velocity time series plots shown have been displaced by 50-m/s increments for March 1, 1983, and 100-m/s increments for March 14, 1983.

8–10 km. The short-period fluctuations exhibited rms velocity variations of up to 50 m/s for data segments of only 17 min in length (Figure 5 and Table 1). These observations pertain to the onset phase of spread $F$.

TABLE 1. Drift Velocity Measurements During Spread F Conditions at Jicamarca, Peru

| Altitude, km | <v>, m/s | σ, m/s | <Δv>, m/s |
|---|---|---|---|
| | March 1, 1983 | | |
| 460 | -70.4 | 25.6 | 38.9 |
| 470 | -78.2 | 27.6 | 32.6 |
| 480 | -79.8 | 22.4 | 22.0 |
| 490 | -91.8 | 20.3 | 32.3 |
| 500 | -81.9 | 18.7 | 10.4 |
| | March 14, 1983 | | |
| 306 | -142.7 | 31.3 | 35.4 |
| 314 | -102.9 | 40.5 | 45.1 |
| 322 | -139.3 | 36.9 | 21.4 |
| 330 | -120.1 | 46.3 | 35.5 |
| 338 | -155.0 | 47.2 | 56.1 |

The negative mean drift velocities denote eastward drift.

The incoherent scatter radar and radar interferometer techniques have also detected deterministic vertical shears in the zonal velocity during the postsunset to premidnight period [Fejer et al., 1985; Kudeki et al., 1982]. These shears are predicted by numerical models of the F-region drifts as well [e.g., Heelis et al., 1974]. Both the observations and models show that the shear is most pronounced below the $F$ region peak, with no significant height dependence above the peak. It should be noted that one interpretation of the "C" shaped plumes observed in Jicamarca radar echoes [McClure et al., 1977] and Altair radar echoes [Tsunoda, 1981] invokes a shear of zonal wind throughout the ionosphere. The scintillation technique is most sensitive to the velocities at the peak of the $F$ layer, however. Thus, it is not clear whether the shear much below or above the peak is detectable with the scintillation technique.

Recently, Basu et al. [1986] used the Briggs method to measure the $V_C$ parameter on two nights during Project Condor. On one occasion they found that $V_C$ was 67 m/s shortly after the onset of scintillation and had fallen to 28 m/s approximately one and a half hours later. These observations are consistent with the trend seen in Figure 4 where the measured values for $V_C$ are seen to decrease rapidly after 2100 LST. Also during Project Condor, while $V_C$ was measured to be 28 m/s with $V_0$ equal to 107 m/s, radar interferometer measurements of fluctuating zonal drift at altitudes corresponding to maximum ionization density at this time (510 to 540

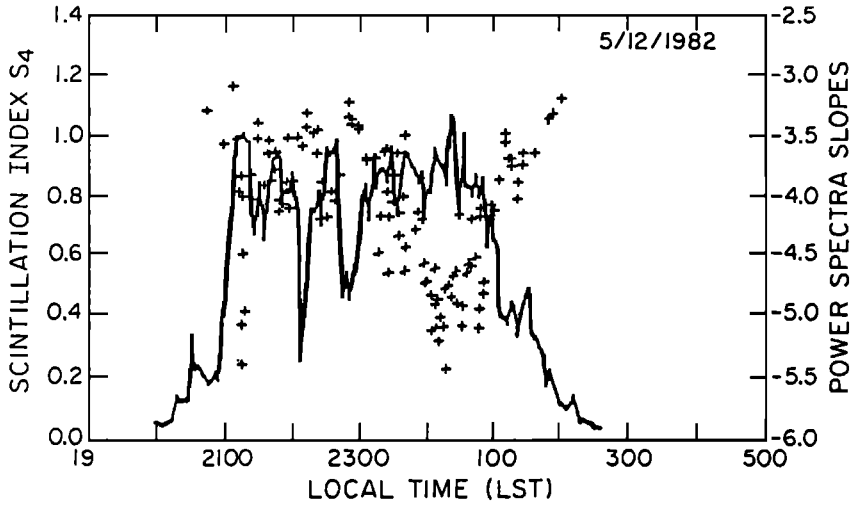


Fig. 6. Measured amplitude power spectra slopes for May 12, 1982. The slopes are denoted by plus signs using the right scale. The scintillation index, $S_4$, using the left scale, is denoted by a continuous line.

km), showed a mean velocity of 114 m/s with an rms fluctuation, $\sigma_v$, of 22 m/s. The two methods seem to be in good agreement at this altitude; however, at topside or bottomside *F* region altitudes, the methods disagree. This is because scintillation measurements are weighted heavily by the levels with high ionization density while the zonal drift possesses considerable variability from bottomside to topside. Therefore it may be concluded that the spaced receiver methods are most sensitive to the rms velocity fluctuations at the altitude range of maximum ionization density along the line-of-sight path.

The amplitude scintillation data were also processed to give spectra as described in section 2. As is usually the case, the amplitude spectrum on a log-log plot shows a corner frequency, below which the spectrum is relatively flat and above which it shows a linear roll-off on the log scale. This roll-off suggests a power law spectral dependence and can be scaled to give the power law spectral index or spectral slopes. In a study by Basu et al. [1980], the spectral slopes were generally observed to steepen after the first hour of scintillation. This suggests the progressive decay of small irregularities. Many days of our scintillation data seem to support this steepening trend. However, there were also days when such steepening did not occur. A case in point is the data of May 12, 1982, the same day as shown in Figure 2.

Figure 6 shows the measured power spectra slopes for May 12, 1982. Except for a notch centered at about 2400 LST, this represents a case where some of the postmidnight slopes do not steepen, but are equal to or even shallower than the early evening slope values. These shallow slopes usually are observed at the westernmost edge of a scintillation patch. This would be in agreement with the findings of McClure et al. [1977], who observed that some bubbles and strong scintillation patches leave "trails" of smaller-sized irregularities.

The postmidnight notch in the spectral slopes as shown in Figure 6 is interesting and has been observed for many nights. To illustrate this phenomenon, many days of data have been analyzed to get a composite plot. Figure 7 shows the measured power spectral slopes for 20 nights of UHF data. Only those data segments with $S_4 \leq 0.5$ have been included in this figure. The gross trend shows an average slope of -3.0 at the onset of scintillation, a gradual steepening due to the decay of the smaller, subkilometer-sized irregularities and then a return to an average value of -3.5 at the edges of strong scintillation patches. On the suggestion of one of the reviewers, we have checked to see whether the shallower slopes observed on some nights in the postmidnight period are associated with magnetically active conditions. This might be expected since it is known that magnetic storm activity correlates with increased incidence of freshly generated bubbles in the postmidnight period [Aarons, 1982]. We do not

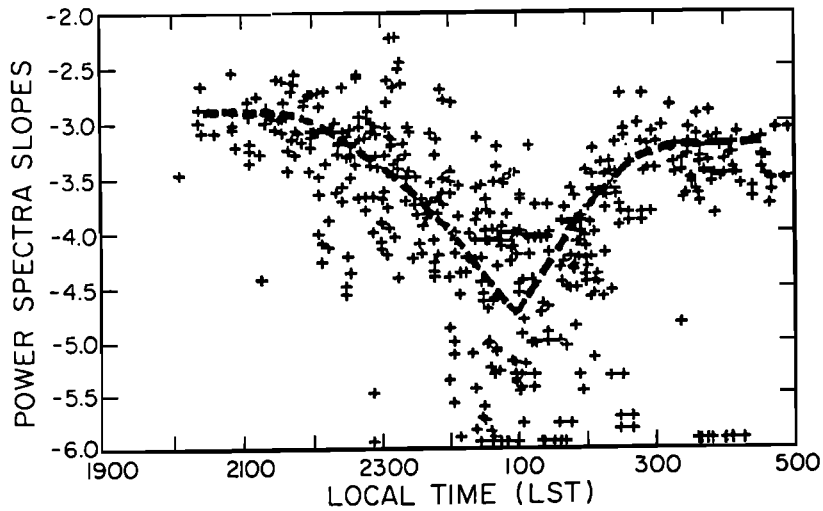


Fig. 7. Measured amplitude power spectra slopes for 20 nights containing weak scintillation data ($0.15<S_4<0.5$). The trend of the measured slopes is also shown.

find that this is an important factor in the cases that we have studied. For example, the data shown in Figures 6 and 8 both show the shallow slopes after midnight, but are associated with magnetically quiet conditions. From observations of both Figures 4 and 7, shallow power spectra slopes and large random velocity components seem to coincide during the onset of spread $F$ phase. However, when weak scintillation theory is used with a locally frozen flow model, the measured power spectra slopes are not found to change as a result of increasing rms fluctuations in the drift velocity distribution of the irregularities.

When scintillation is considered to be strong or for this analysis when the scintillation index value exceeds 0.5, the 50% autocorrelation time is used as a measure of the changes in the mean drift velocity and/or the scattering strength of the irregularities [Basu and Whitney, 1983]. Based on this hypothesis, the measured 50% autocorrelation times and mean drift velocity values can be used to determine the effect that increased scattering strength of the irregularities has on the UHF and $L$ band power spectra shapes and roll-off slopes. This is demonstrated by the scintillation data of May 6, 1982. For this day, the spaced receiver data at UHF have been analyzed for the drift, the autocorrelation time, the scintillation index and the spectral slopes. The $L$ band data have been analyzed for the scintillation index and the spectral slopes. The results are shown in Figure 8. On this night the postmidnight scattering strength becomes so great that even the $L$ band $S_4$ index reaches values as high as 0.6. The postmidnight drift velocity remained relatively constant at 100 m/s and the cross-correlation coefficient remained between 0.95 and 1.0. The top panel of Figure 8 depicts a dip of correlation times at 2430 LST. This dip in correlation times is accompanied by a steepening of UHF spectral slopes shown in the middle panel and by a steepening of $L$ band spectral slopes shown in the bottom panel, but not by any sudden increase in the drift velocity. These data seem to suggest that the temporal decorrelation of the scintillation at UHF is caused both by the saturated scintillation and a steepening of the irregularity spectrum. This is supported by Figure 9 which shows the measured UHF and $L$ Band spectra at the peak of the estimated increase in the scattering strength of the irregularities. The UHF spectra near the roll-off frequency are no longer a power law form but rather resemble a Gaussian form. This guassian form is also consistent with the "strong focusing" scintillation modeling done by Franke and Liu [1984]. Because of the nonpower law form near the spectrum roll-off frequency, the linear slopes calculated for these spectra become highly variable (usually between -5.0 and -6.5). The $L$ band power spectrum at this time is also steeply sloped, but since the $S_4$ index is only ~0.6, it is likely that this steepening is due to a change in the irregularity spectrum and not to strong scattering effects.

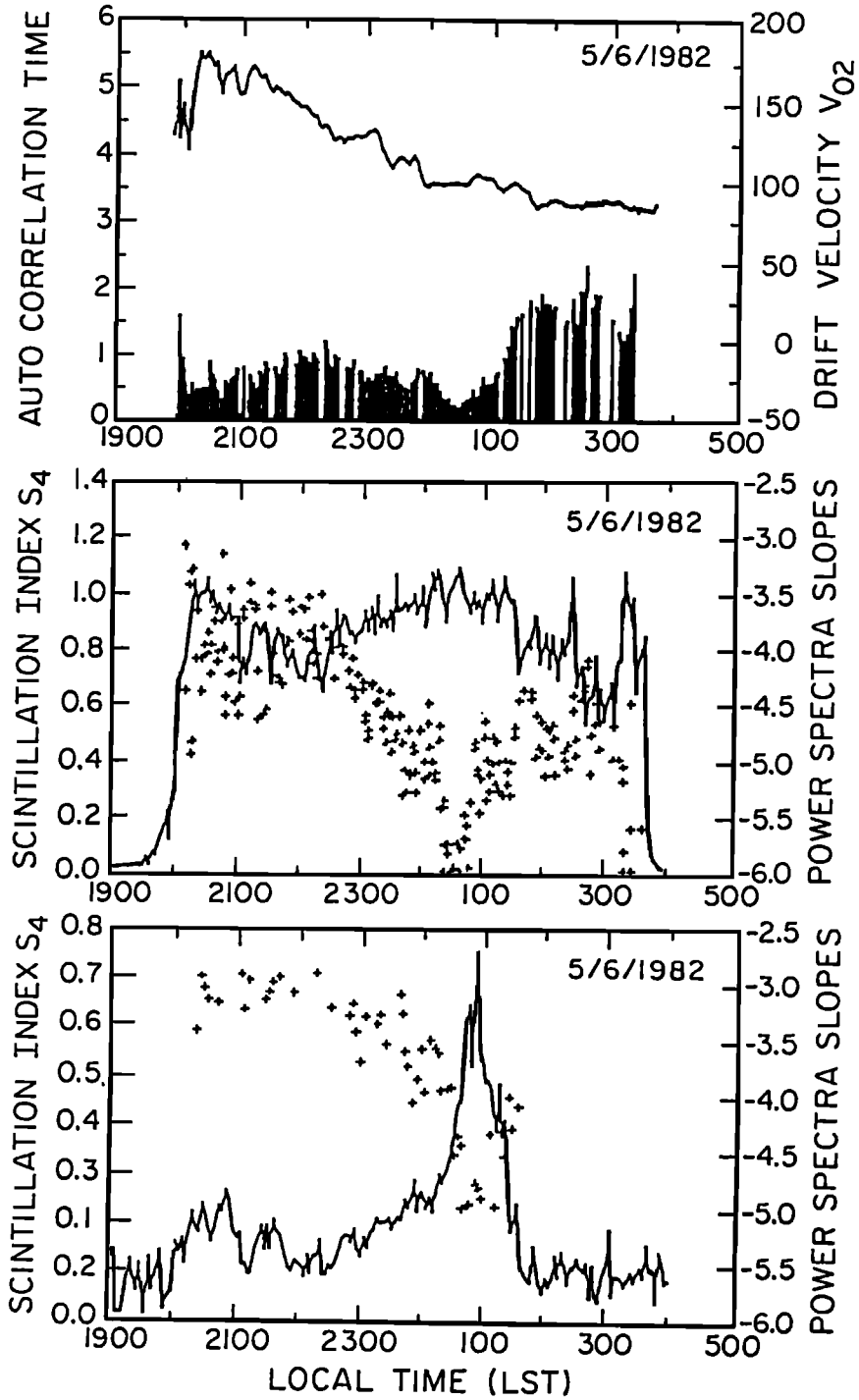


Fig. 8. The scintillation data for May 6, 1982. The top panel shows the autocorrelation times (vertical lines, left scale) and the drift velocities (continuous curve, right scale); the middle panel shows the scintillation index $S_4$ (continuous curve, left scale) and the power spectral slopes (denoted by plus signs, right scale), all derived from the UHF data. The lower panel shows the $L$ band scintillation index $S_4$ (continuous curve, left scale) and the $L$ band spectral slopes (denoted by plus signs, right scale).

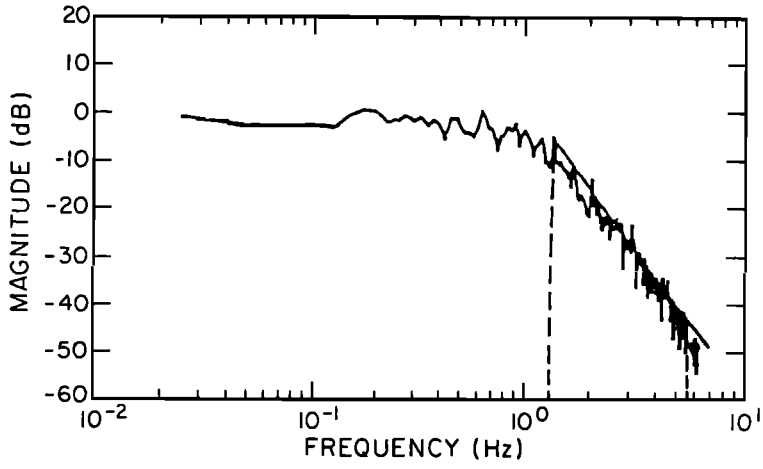


POWER SPECTRUM
GUAM, EAST RECEIVER (CHO)
DATE: 5/6/1982
START TIME (LST): 24:19:2.0

SLOPE = -6.1780 +/- 0.1833
CORRELATION TIME (sec) = 0.281
FREQUENCY RESOLUTION = 0.0244
$S_4$ INDEX = 1.0380

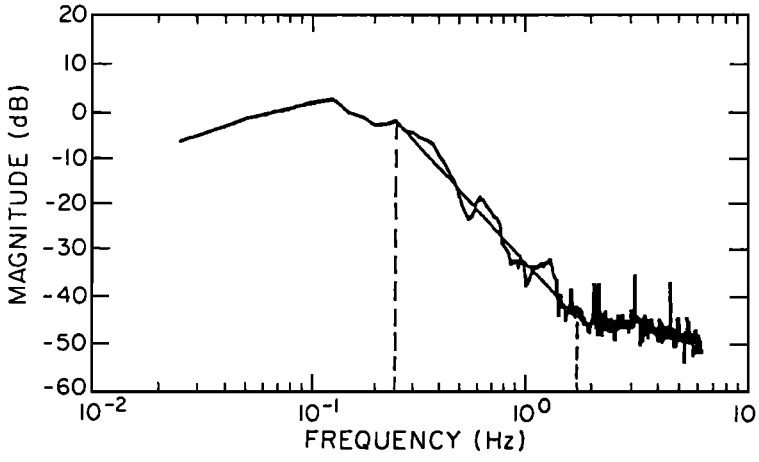


POWER SPECTRUM
GUAM, L-BAND RECEIVER (CH2)
DATE: 5/6/1982
START TIME (LST): 24:30:20

SLOPE = -5.0891 +/- 0.1700
CORRELATION TIME (sec) = 1.001
FREQUENCY RESOLUTION = 0.0244
$S_4$ INDEX = 0.6322

Fig. 9. Measured amplitude power spectra from the night of May 6, 1982. The first spectrum corresponds to saturated scintillation of the UHF signal and the second corresponds to the received $L$ band signal at about the same time near the dip of correlation time shown in Figure 8.

## 4. CONCLUSIONS

From this analysis, some interesting aspects of ionospheric $F$ region irregularities and their effect on both UHF and $L$ band radio signals were uncovered. Using two spaced receivers aligned in the magnetic east-west direction, the mean drift velocity of equatorial irregularities was calculated. Three spaced receiver correlation methods were used to determine the mean drift velocity and all three methods were in reasonable agreement. Drift velocities as high as 200 m/s in a magnetic eastward

direction just after local sunset were calculated on a few nights, but on most nights an average drift velocity of 120 to 150 m/s was observed. The drift velocities tended to decrease gradually from after local sunset until the end of scintillation activity.

In addition to the mean drift velocity, the characteristic random velocity was also calculated using each of the three correlation methods. The three methods also seemed to be in agreement as to the decaying trend observed in the magnitude of the random velocity. This trend was first reported by Vacchione et al. [1987]. The period of time from local sunset to one or two hours later was observed to have the highest random velocity values. As the night progressed, the random velocity decreased rapidly, with slight increases observed at the walls of scintillation patches. Thus, the increases in $V_C$ near the edges of scintillation patches could be caused by enhanced vertical shear in the zonal velocity, or enhanced fluctuating components of the vertical and/or horizontal velocities. The random velocity is interpreted as being directly a measure of the width of the drift velocity distribution along the path and over the measurement interval at the altitude of maximum ionization density. It is at this altitude that the UHF signal appears to be most affected because of the strength of this region's irregularities. This interpretation is based on weak scintillation modeling. Unfortunately, because of the slanted line-of-sight paths of the UHF signals, the separate contributions of horizontal and vertical drift fluctuations could not be distinguished through the use of these spaced receiver data alone.

Power spectra of the amplitude fluctuations were calculated during times of strong and weak scintillation. The slopes of the spectra roll-off for weak scintillation cases were determined to steepen from the postsunset to postmidnight periods. Using weak scintillation theory and the calculated drift velocity values, this is interpreted to mean the irregularities in the scale size range of 500 m to 1 km have decayed leaving only the larger, kilometer-sized irregularities in the post midnight period. There were exceptions to this decaying trend and those usually occurred at times when a strong scintillation patch had already passed through the signal paths and shallow slopes were observed at the patch's western edge. This was interpreted to be the trail of smaller-sized irregularities left behind by strong scintillation patches.

As UHF scintillation became strong, the 50% autocorrelation times were used as measures in the changes of the scattering strength of the irregularities and/or their mean drift velocity. Since the mean drift velocities were calculated, long periods when the drift velocity remained relatively constant were analyzed to determine the effect that changing scattering strength had on the UHF and $L$ band power spectra. From observations of the UHF and $L$ band power spectra measured at this time, the increasing scattering strength of the irregularities was observed to cause steepening of the power spectra slopes. When the scattering strength increased to a point where the scintillation index values reached saturation, the UHF power spectra resembled a Gaussian form at the roll-off frequencies.

Some power spectra slopes, calculated during times of strong scintillation, were observed to follow the same decaying trend as those spectra slopes measured during weak scintillation. This is interpreted to mean the decaying process of the smaller-sized irregularities could be observed even during moderately strong scintillation periods. This would indicate that the simple relationship between the power spectrum slope and the irregularity scale size distribution may still be valid during times of moderately strong scintillation if no increases in the scattering strength of the irregularities are detected.

*Acknowledgments.* Partial support from the Atmospheric Sciences Division of the National Science Foundation under grant ATM 84-14134 is acknowledged with pleasure. We wish to express sincere thanks to M. R. Paulson of the Naval Ocean Systems Center in San Diego for supplying the high-quality data tapes.

## REFERENCES

Aarons, J., Equatorial scintillations: A review, *IEEE Trans. Antennas Propag., AP-25*, 729–736, 1977.

Aarons, J., Global morphology of ionospheric scintillations, *Proc. IEEE, 70*, 360–373, 1982.

Basu, S., and H. E. Whitney, The temporal structure of intensity scintillations near the magnetic equator, *Radio Sci., 18*, 263–271, 1983.

Basu, S., S. Basu, J. Aarons, J. P. McClure, and M. D. Cousins, On the coexistence ofkilometer- and meter-scale irregularities in the nighttime equatorial F region, *J. Geophys. Res., 83*, 4219–4226, 1978.

Basu, S., J. P. McClure, S. Basu, W. B. Hanson, and J. Aarons, Coordinated study of equatorial scintillation and in situ and radar observations of nighttime F region irregularities, *J. Geophys. Res., 85*, 5119–5130, 1980.

Basu, S., S. Basu, J. LaBelle, E. Kudeki, B. G. Fejer, M. C. Kelley, H. E. Whitney, and A. Bushby, Gigahertz scintillations and spaced receiver drift measurements during Project Condor

equatorial *F* region rocket campaign in Peru, *J. Geophys. Res.*, *91*, 5487–5526, 1986.

Briggs, B. H., G. J. Phillips, and D. H. Shinn, The analysis of observations on spaced receivers of the fading of radio signals, *Proc. Phys. Soc. London, Sect. B*, *63*, 106–121, 1950.

Coles, W. A., and S. Maagoe, Solar wind velocity from IPS observations, *J. Geophys. Res.*, *77*, 5622–5624, 1972.

Fejer, B. G., E. Kudeki, D. T. Farley, Equatorial *F* region zonal plasma drifts, *J. Geophys. Res.*, *90*, 12,249–12,255, 1985.

Franke, S. J., and C. H. Liu, Analysis and simulation of multi-frequency equatorial scintillation, *Tech. Rep. 70*, Ionos. Radio Lab., Univ. of Ill. at Urbana-Champaign, 1984.

Heelis, R. A., P. C. Kendall, R. J. Moffett, D. W. Windle, and H. Rishbeth, Electrical coupling of the E and F regions and its effect on *F* region drifts and winds, *Planet. Space Sci.*, *21*, 743, 1974.

Kudeki, E., and S. J. Franke, Radar interferometer estimate of zonal drift variability during spread *F*, *Geophys. Res. Lett.*, *13*, 1117–1120, 1986.

Kudeki, E., B. G. Fejer, D. T. Farley, and H. M. Ierkic, Interferometer studies of equatorial *F* region irregularities and drifts, *Geophys. Res. Lett.*, *9*, 337, 1982.

McClure, J. P., W. B. Hanson, and J. H. Hoffman, Plasma bubbles and irregularities in the equatorial ionosphere, *J. Geophys. Res.*, *82*, 2650–2656, 1977.

Ossakow, S. L., Spread *F* theories: A review, *J. Atmos. Terr. Phys.*, *43*, 437–452, 1981.

Paulson, M. R., Daytime equatorial scintillation of satellite signals at Guam, in *Effect of the Ionosphere on $C^3$ I Systems*, edited by J. M. Goodman, pp.179–185, U. S. Government Printing Office, Washington, D.C., 1984.

Tsunoda, R. T., Time evolution and dynamics of equatorial backscatter plumes, 1, Growth phase, *J. Geophys. Res.*, *86*, 139–149, 1981.

Vacchione, J. D., S. J. Franke, and K. C. Yeh, A new analysis technique for estimating zonal irregularity drifts and variability in the equatorial *F* region using spaced receiver scintillation data, *Radio Sci.*, *22*, 745–756, 1987.

Valladares, C. E., W. B. Hanson, J. P. McClure, and B. L. Cragin, Bottomside sinusoidal irregularities in the equatorial *F* region, *J. Geophys. Res.*, *88*, 8025–8042, 1983.

Welch, P. D., The use of the fast Fourier transform for the estimation of power spectra: A method based on time averaging over short, modified periodograms, *IEEE Trans. Audio Electracoust*, *AU-15*, 70–73, 1967.

Wernik, A. W., C. H. Liu, and K. C. Yeh, Modeling of spaced receiver scintillation measurements, *Radio Sci.*, *18*, 743–764, 1983.

Woodman, R. F., Vertical drift velocities and east-west electric fields at the magnetic equator, *J. Geophys. Res.*, *75*, 6249–6259, 1970.

S. J. Franke, D. E. Spatz, and K. C. Yeh, Department of Electrical and Computer Engineering, University of Illinois at Urbana-Champaign, 1406 West Green Street, Urbana, IL 61801.